

## 28. STRUCTURAL IMPLICATIONS OF GRAVITY ANOMALIES, RESOLUTION AND HEEZEN GUYOTS, MID-PACIFIC MOUNTAINS<sup>1</sup>

William W. Sager<sup>2</sup>

### ABSTRACT

Drilling showed that carbonate rocks make up most of Resolution Guyot, located in the western Mid-Pacific Mountains. Density data from Hole 866A, in the top of the guyot, were used to calculate a forward model of the gravity anomaly caused by the guyot's topography. After this anomaly was subtracted from the observed free-air anomaly, a significant positive residual, 35 mGal in amplitude, remained. The same densities were used for nearby Heezen Guyot, which yielded a similar, 45 mGal residual. Inverse models of the Resolution Guyot residual indicate that most of the mass excess can be attributed to the contrast between surrounding sediments and the dolomites at the bottom of the guyot's limestone section and the basalt pedestal beneath the guyot. Nevertheless, models with a central mass concentration fit the residual significantly better than those without, suggesting that there may be either a buried, conical, seamount remnant in the center of the guyot or a central conduit with dense intrusive rocks. The latter seems more plausible because seismic reflection profiles show no evidence of a buried conical structure. In addition, models with bottoms below the predicted top of the underlying basaltic plateau give more plausible density contrasts, suggesting that either a dense zone exists within the plateau beneath the guyot or that the extrapolated depth to the plateau top is incorrect by 500 m to 1000 m. The Resolution Guyot models imply that the carbonate bank buried a small seamount or igneous pedestal and retained nearly the same shape and width. Although the Heezen Guyot residual anomaly was not explicitly modeled, it is similar to that of Resolution Guyot and implies an analogous subsurface structure. In contrast, the Heezen Guyot residual is located to the west side of that edifice and does not have the same elongated shape as the guyot. Thus, it appears that the carbonate bank of Heezen Guyot expanded eastward from its pedestal.

### INTRODUCTION

Ocean Drilling Program (ODP) Hole 866A was drilled into the top of Resolution Guyot in the Mid-Pacific Mountains. A surprise result was that all of the buildup above the surrounding seafloor consists of carbonate rock. The guyot sits atop a basaltic plateau, approximately 1 km in height, that underlies many of the Mid-Pacific Mountains seamounts (Winterer and Metzler, 1984). Consequently, if a volcanic construct rises from the plateau beneath the guyot, it must be small, perhaps only 500 m in height (Sager, Winterer, Firth, et al., 1993).

Both magnetic and gravity data were collected over Resolution Guyot and nearby Heezen Guyot (Fig. 1) during pre-drilling site surveys. Their magnetic anomalies imply a magnetic contrast beneath each guyot, as might be expected from a basalt cone buried by nonmagnetic carbonate rock; however, their gravity anomalies likely result primarily from the contrast between carbonate rock and seawater. Drilling at Site 866, during Leg 143, and nearby Site 463, during DSDP Leg 63, provided a detailed profile of density through the top of Resolution Guyot and the sediments that surround it. With these data it is possible to use gravity modeling techniques to calculate the effects of known density contrasts and elucidate the deeper structure. In this chapter, I describe the results and implications of gravity modeling for Resolution and nearby Heezen guyots.

### Geologic Setting

Resolution and Heezen guyots are located in the western Mid-Pacific Mountains province, approximately 100 km apart, and are similar to many other guyots in the region. Resolution Guyot is sub-circular in plan view and has a flat summit platform about 25 km in diameter at a depth of approximately 1300 m (Fig. 2). Heezen Guyot has a similar platform at nearly the same depth, but the edifice is

kidney-shaped, approximately 12 km in width by 20 km in length (Fig. 3). Both guyots are located in an area of shallow seafloor, with a depth of about 2500 to 3000 m, as compared to the abyssal seafloor depths (5100–5500 m) of the Mesozoic seafloor in the region surrounding the Mid-Pacific Mountains (Fig. 1). The regions of shallower seafloor appear to be a low basaltic plateau, about 1 km in height, which is topped by guyots and as much as about 1 km of sediment (Winterer and Metzler, 1984). Resolution Guyot is located in the middle of an area of shallower seafloor and the deepest depths on its flanks are only about 3000 m (Figs. 1, 2). Heezen Guyot is located near the edge of this platform, so depths on its east side are much shallower than those on its west (Figs. 1, 3).

The age of the lithosphere beneath the Mid-Pacific Mountains in the vicinity of Resolution and Heezen guyots is somewhat uncertain, but magnetic anomaly lineations extrapolated from the surrounding area suggest an Early Cretaceous age of about 130 Ma (Sager, Winterer, Firth, et al., 1993). <sup>40</sup>Ar–<sup>39</sup>Ar radiometric dates of basalts drilled from Hole 866A average 126 Ma (Pringle, this volume), indicating that the igneous basement beneath the guyot formed soon after the lithosphere. It is thought that the age of the plateau beneath the guyots is approximately the same age (Sager, Winterer, Firth, et al., 1993).

### Constraints from Drilling

DSDP Site 463 is located 44 km to the northeast of Resolution Guyot at a depth of 2525 m (Fig. 1; Thiede, Vallier, et al., 1981). The hole penetrated 823 m of sediments, but did not strike basement. From a single-channel seismic reflection line over Site 463 collected during the site-survey cruise, basement has been extrapolated to be another 150 to 200 m deeper, at about 1000 meters below the seafloor (mbsf) or 3525 meters below sea level (mbsl) (Sager, Winterer, Firth, et al., 1993). This may be the level of the top of the plateau beneath the guyots.

Hole 463 penetrated a succession (proceeding downward) of nanofossil ooze overlying nanofossil chalk overlying limestones and limestones interbedded with volcanoclastics (Fig. 4). Discrete sample

<sup>1</sup> Winterer, E. L., Sager, W. W., Firth, J. V., and Sinton, J. M. (Eds.), 1995. *Proc. ODP, Sci. Results*, 143: College Station, TX, (Ocean Drilling Program).

<sup>2</sup> Departments of Oceanography and Geophysics, Texas A&M University, College Station, TX 77843-3146, U.S.A.

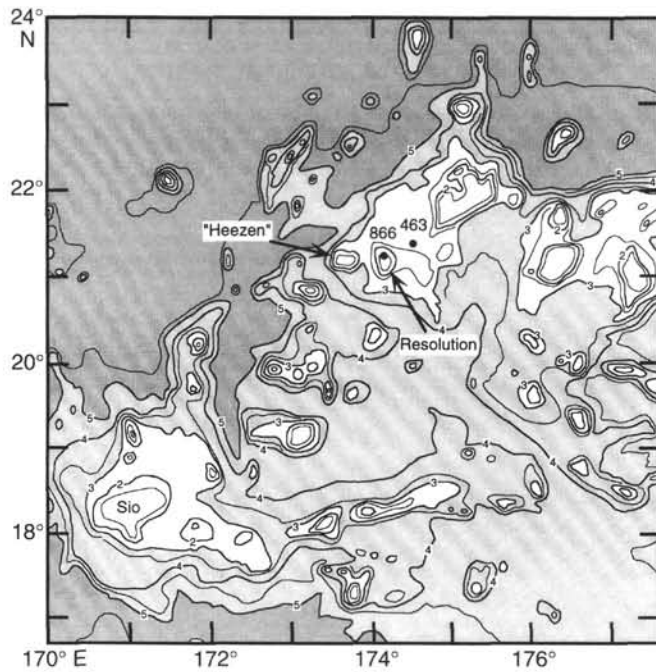


Figure 1. Generalized bathymetry chart of the western Mid-Pacific Mountains, showing the locations of guyots examined in this study or mentioned in the text. Locations of DSDP Site 463 and ODP Site 866 shown as solid dots. Bathymetry redrawn from Mammerickx and Smith (1985); contours at 500 m intervals, with heavy contours at 1 km intervals. Contour labels in kilometers.

density measurements from core samples show an average of about  $1800 \text{ kg m}^{-3}$  above 450 mbsf and  $2300 \text{ kg m}^{-3}$  below (Thiede, Vallier, et al., 1981).

Hole 866A was drilled about 1.1 km inward from the northern edge of the summit platform of Resolution Guyot (Sager, Winterer, Firth, et al., 1993). Starting at a depth of 1362 m, it penetrated a thin pelagic cover overlying 1620 m of shallow-water limestones and 124 m of subaerial basalts. Thus, basement beneath the guyot is at a total depth of 2982 m at the location of Site 866.

The limestones at Site 866 are Early Cretaceous in age and range from Barremian to Albian age. In general, they are porous, with moldic porosity, except for two zones where extensive diagenesis has occurred. The first of these is lithologic Subunit IIIC (271.0–434.5 mbsf; Fig. 4), a zone of higher-than-average density containing mudstone-wackestone with calcareous horizons. The other encompasses Units VII and VIII, a zone of extensive dolomitization that extends from 1203.4 mbsf to near basement at 1601.3 mbsf (Sager, Winterer, Firth, et al., 1993).

The wireline bulk density log shows a general increase with depth through the limestone section, from approximately  $2100 \text{ kg m}^{-3}$  at the surface to  $2600 \text{ kg m}^{-3}$  at the basalt contact (Fig. 4; Sager, Winterer, Firth et al., 1993). The exception to this trend is Subunit IIIC, which shows higher, variable densities of 2200 to  $2700 \text{ kg m}^{-3}$ .

Discrete sample bulk density measurements generally correlate with the log measurements, but are often slightly higher because denser rocks are more likely to be recovered in the cores. Discrete sample densities in the upper 400 mbsf (Units II and III) range from 2400 to  $2700 \text{ kg m}^{-3}$ . Directly below, densities are less, about  $2200 \text{ kg m}^{-3}$ , but increase linearly downward to  $2600 \text{ kg m}^{-3}$  at 1200 mbsf. In the dolomitized zone between 1200 mbsf and basement, discrete sample bulk densities vary systematically back and forth from 2100 to  $2800 \text{ kg m}^{-3}$ , evidently through alternating hard and soft layers.

Only a short section of basalt was cored, and it displayed a large variation in character. The basalts were subaerial flows, with dense centers, vesicular or fractured edges, and clay zones between (Sager,

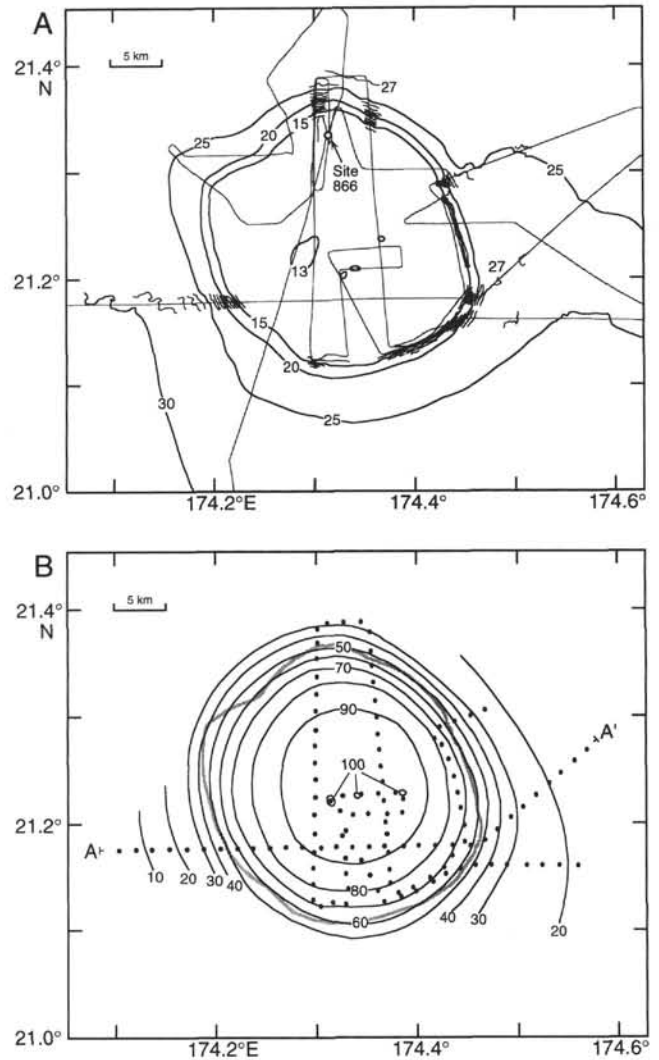


Figure 2. Bathymetry (A) and free-air gravity anomaly (B) maps of Resolution Guyot. Bathymetry contours are shown at 500-m intervals, except where SeaBeam multibeam echo-sounder contours are shown at 100-m intervals. Bathymetry contours are labeled in hundreds of meters. Light gray lines show ship tracks. Gravity contours are shown at 10-mGal intervals and are labeled in mGals. A heavy gray contour shows the 2000-m bathymetry contour for reference. Dots show location of gravity data points used for modeling; "A" and "A'" show the beginning and end points of the profile shown in Figures 8 and 9.

Winterer, Firth, et al., 1993). As a consequence of these lithologic variations, the densities in both wireline logs and discrete measurements were extremely variable. Wireline log bulk densities ranged from 1800 to  $2800 \text{ kg m}^{-3}$ , whereas most discrete measurements varied from 2300 to  $2900 \text{ kg m}^{-3}$  (Fig. 4).

The short length of the cored basalt section and its wide variability of density values poses a problem for accurate modeling. Most investigators who have modeled the gravity anomalies of basaltic seamounts have arrived at average densities between 2500 and  $2700 \text{ kg m}^{-3}$  (LePichon and Talwani, 1964; Schimke and Bufe, 1968; Sager et al., 1982; Kellogg and Ogujiofor, 1985; Kellogg et al., 1987; Freitag, 1987). Consequently, a value of  $2600 \text{ kg m}^{-3}$  was used here because it is in the middle of the range of observed density values (Fig. 4) and mean density results for seamounts. One implication of this density value is that there is little expected density contrast between the basalt and overlying dolomites (approximately  $100 \text{ kg m}^{-3}$ ) or relative to the surrounding limestones ( $300 \text{ kg m}^{-3}$ ).

## BATHYMETRY AND GRAVITY DATA

Geophysical data were collected over both guyots during the Roundabout Expedition, Leg 10, aboard the *Thomas Washington* in December 1988. Heezen Guyot was the more extensively surveyed, with many lines run around and over its summit and lines run down the flanks in all quadrants (Fig. 3). Resolution Guyot was only partially surveyed, but had lines run across the summit in east-west and north-south directions, as well as flank lines to the east and south (Fig. 2). Additional bathymetry data were collected over Resolution Guyot aboard the *JOIDES Resolution* during Leg 143, in part to fill gaps in the Roundabout survey.

Bathymetry data were obtained with a SeaBeam multibeam echosounder during the Roundabout cruise. This device insonifies a swath having a width of about 75% of the water depth and has a depth precision of about 10 m. During Leg 143, depths were measured with a 3.5 kHz echo-sounder, which should have a precision of less than 10 m in areas where the seafloor slope is not steep. For both data sets, an acoustic wave velocity of  $1500 \text{ ms}^{-1}$  was assumed in seawater, and no corrections were made for variations with depth. Errors of several tens of meters could result from not making such corrections, but they should have an insignificant effect on the gravity modeling results.

Gravity measurements were made with a Bell-Aerospace BGM-3 marine gravimeter mounted on a gyro-stabilized platform. The precision and capabilities of this meter are described by Bell and Watts (1986). Its design eliminates cross-coupling errors that affect other marine gravimeters. Although it is capable of submilliGal precision ( $1 \text{ mGal} = 10^{-5} \text{ ms}^{-2}$ ), its accuracy and precision are limited by navigation errors that cause errors in the Eötvös correction, as well as differences at the ship's track crossover points.

Navigation data were recorded once per minute from Transit satellite and global positioning system (GPS) receivers, as well as from pit, gyrocompass, and Doppler speed logs. GPS is by far the most accurate of the navigation systems, with an accuracy of less than 100 m, but reliable GPS satellite coverage was only available for 8 to 10 hr/day. Thus, GPS was used for navigation fixes whenever it provided reliable data, and Transit satellite fixes connected by dead reckoning were used to fill the gaps. Although Transit satellite fixes typically have inaccuracies of 500 m or more, the SeaBeam multibeam echosounder data were used to correct for navigation errors at the ship's track crossover points.

A measure of the gravity data precision is given by ship's track crossover errors. The Resolution Guyot survey has a mean crossover error of 1.3 mGal, whereas the Heezen survey mean error is 3.6 mGal. These errors appear random and are only a few percent of the total amplitude of either guyot's gravity anomaly; thus, they were not considered a significant factor in modeling.

Free-air gravity anomaly maps were prepared for each guyot at a contour interval of 10 mGal. Resolution Guyot has a subcircular anomaly, with an amplitude of about 100 mGal (Fig. 2B). The free-air anomaly of Heezen Guyot is elongated in the direction of the guyot's bathymetric long-axis and has a value over the summit of about 100 mGal, similar to Resolution Guyot (Fig. 3B). However, over the west flank of the guyot, where seafloor depths are greater than on the east, the anomaly reaches low values of  $-40 \text{ mGal}$ .

## GRAVITY MODELING

The goal of this study was to use the density data provided by drilling at Site 866 to calculate the gravity anomaly of the limestone buildup of Resolution Guyot, to remove its effect from the observed anomaly, and to model the remainder for its constraints on deeper structure. Although no density data are available for Heezen Guyot, its proximity and the similarity of size, depth, and morphology suggested a similar density structure could be used to model its topographic expression.

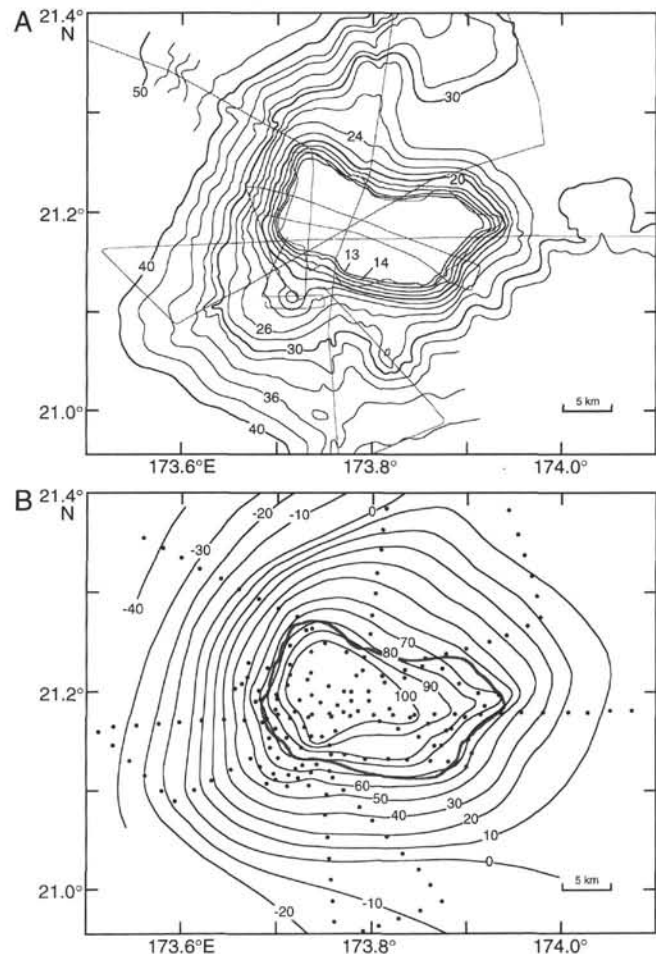


Figure 3. Bathymetry (A) and free-air gravity anomaly (B) maps of Heezen Guyot. Bathymetry contours are shown at 200-m intervals. Conventions are as in Figure 1.

A forward model was used to calculate the gravity effect of the topographic expression of each guyot. The modeling routine of Plouff (1976) was used to represent the bathymetry. This routine approximates the shape of bodies with a stack of vertical-sided prisms, each polygonal in plan view and having a homogeneous density contrast. Bathymetry contours constrained the shapes of the prisms. The resulting forward model was subtracted from the observed free-air anomaly and the residual was subsequently modeled. Several types of subsurface density models, with different shapes and dimensions, were constructed and their mean densities were determined by linear least-squares inversion.

For the forward model of Resolution Guyot, three prisms were used, following the 1500, 2000, and 2500 m contours (Fig. 5). The uppermost prism represented the upper 400 m of the carbonate uplift. Within this portion of Hole 866A, the densities in the upper 200 m are about  $2100$  to  $2200 \text{ kgm}^{-3}$ , whereas those in the lower 200 m are  $2300$  to  $2600 \text{ kgm}^{-3}$ ; thus, a mean density contrast of  $1350 \text{ kgm}^{-3}$  (vs.  $1027 \text{ kgm}^{-3}$  for seawater) was used for this prism. Densities decrease below 400 mbsf, so a mean density contrast of  $1300 \text{ kgm}^{-3}$  was used for the middle layer, which had a thickness of 500 m. The lowest layer was assigned a density contrast of  $1500 \text{ kgm}^{-3}$ . Its bottom was set at 2650 m, the depth of the seafloor on the east side of the guyot (Fig. 2).

Five types of density anomalies were used to model the residual anomaly: (1) the carbonate uplift; (2) a vertical, cylindrical pedestal; (3) a cylinder with a conical top; (4) a deeper, conical structure; and (5)

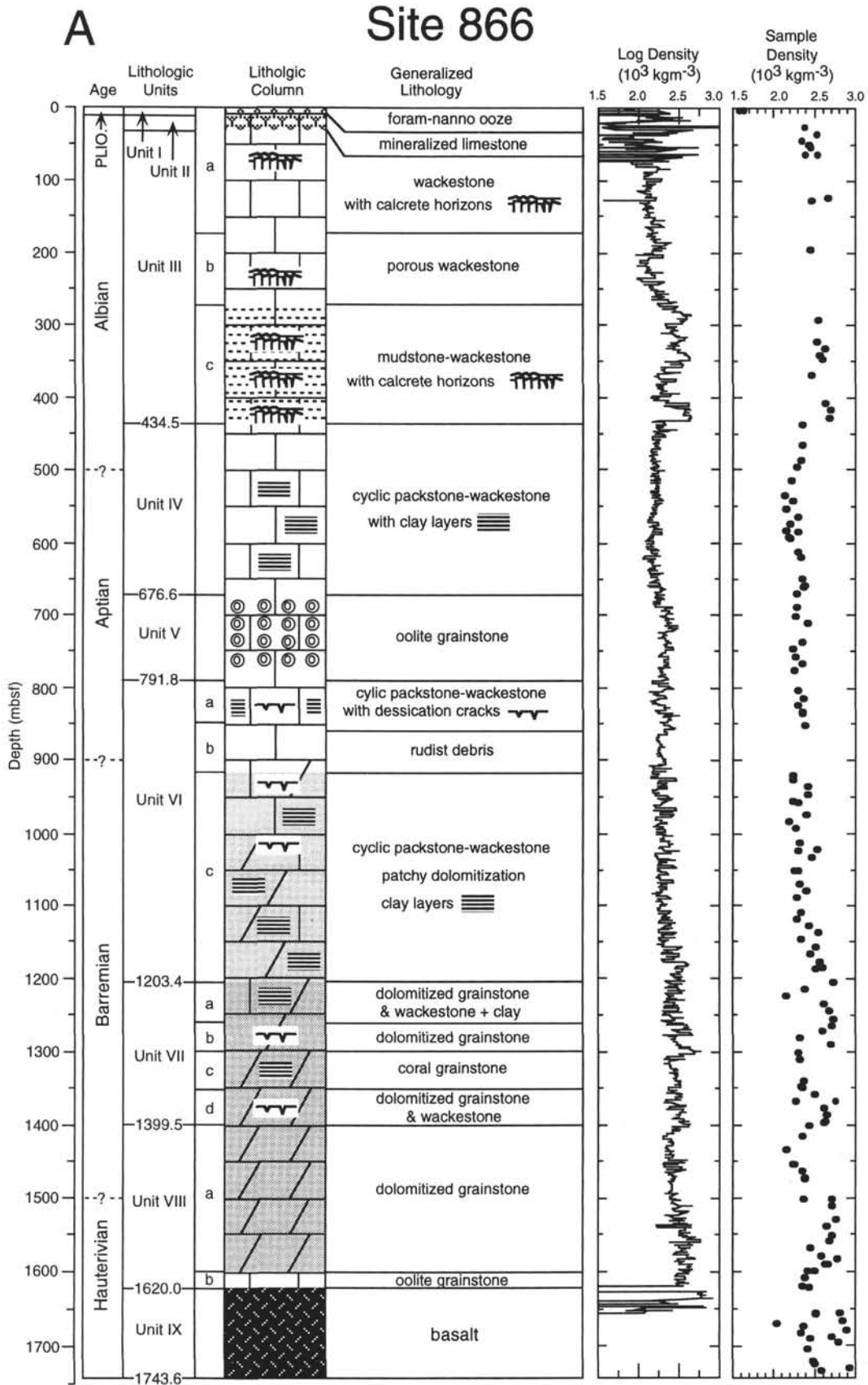


Figure 4. Density and geologic constraints for gravity modeling of Resolution Guyot. **A.** Lithologic column for Site 866, in the summit of the guyot. Age, lithologic units, and generalized lithology are shown at left; gray shows the dolomitized zone. Density measurements from wireline logs and discrete samples are shown at right (Sager, Winterer, Firth, et al., 1993). **B.** Lithologic column for Site 463, on the flanks of the guyot (Thiede, Vallier, et al., 1981). Conventions as in A. C. Cartoon geologic cross section showing the relationships of Sites 866 and 463 and the lithologic units. Vertical exaggeration is approximately 7:1.

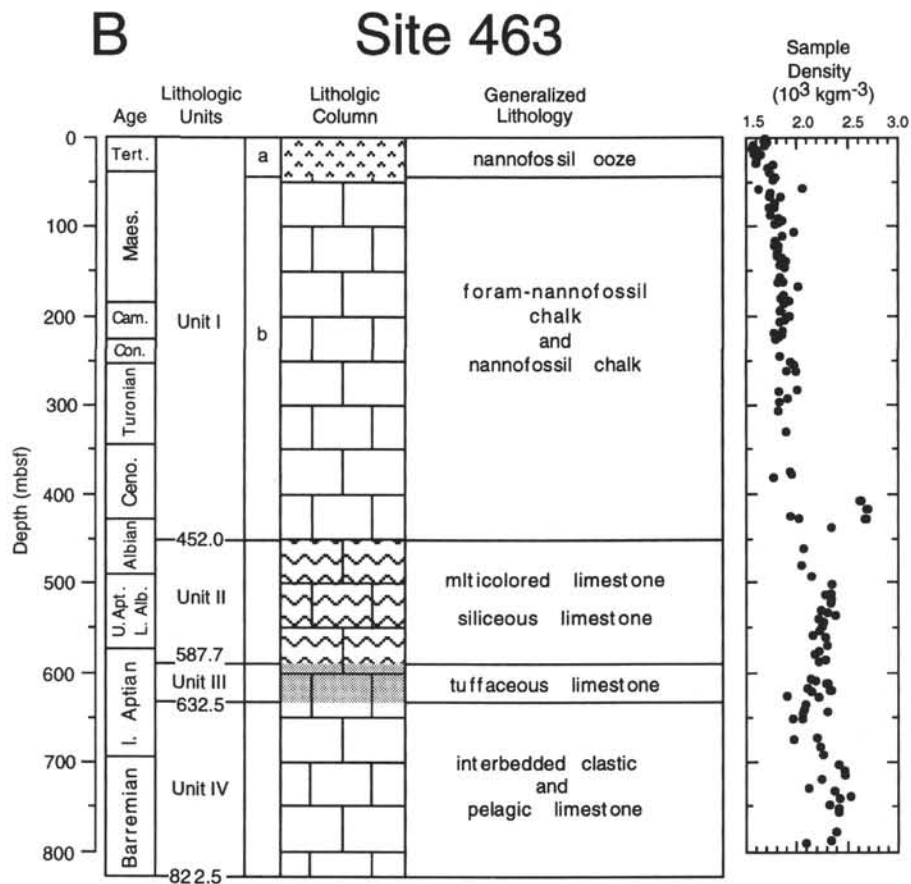


Figure 4 (continued).

a cylindrical pedestal with a dense conduit at its center (Table 1). The shape of the buried cone and cylinders were constructed to follow the shape of the residual anomaly, which is subcircular (Fig. 6). For each model type, different top and bottom depths were tried in an attempt to make a better fit between observed and calculated anomalies.

Model errors were compared using the "goodness-of-fit" ratio (GFR), which is the mean of observed anomaly values divided by the mean of the error (observed minus calculated anomalies) values. Larger GFR values indicate a better fit of calculated with observed anomalies; for example, a GFR of 4.0 implies that 80% of the observed anomaly can be explained by the model. To test for significance differences among models, variances were calculated from the error values. Assuming the errors have a Gaussian distribution, variance ratios can be used to compare models using an F-test (Bevington, 1969).

Because the topography of Heezen Guyot is better defined by bathymetric data, more thinner prisms were used for the forward model of its gravity effect (Fig. 7). However, the density structure within the guyot is unknown, so a simple average density contrast of  $1450 \text{ kgm}^{-3}$  was used for all layers. The model top and bottom were at 1300 and 3200 m, respectively. This model bottom is deeper than that of Resolution Guyot, because the shallowest seafloor surrounding Heezen Guyot is deeper, so it is possible to remove the gravitational effect of a taller topographic buildup. Although the bottom of the forward model is about 200 m beneath the depth of igneous basement drilled at Resolution Guyot, the depth of basement beneath Heezen is unknown and the error caused by assigning a limestone density to basalt should be small owing to their small difference in mean density (Fig. 4). Because the residual anomaly of Heezen Guyot is similar to that of Resolution Guyot, and density structure con-

straints are lacking, no attempt was made to model the Heezen Guyot residual anomaly because similar results were expected.

## RESULTS OF MODEL

Forward models of Resolution and Heezen guyots produced anomalies of 65 and 120 mGal, respectively (Figs. 5, 7). For both guyots, significant residuals were left after subtracting these calculated anomalies from the observed free-air anomalies. The Resolution Guyot residual has an amplitude of about 35 mGal (Figs. 6, 8), whereas that of Heezen Guyot is slightly greater than 45 mGal (Fig. 7). Both residuals are positive and subcircular, indicating a mass excess beneath each guyot. The Resolution Guyot anomaly is centered over the carbonate uplift, but that of Heezen Guyot is offset to the west side of that feature.

Residual Models A1 through A4 attempt to explain the residual anomaly by the carbonate uplift that forms the guyot above the seafloor, or some portion of this body (Fig. 9). The purpose of this model was to determine whether the residual could be the result of an inappropriate density contrast employed in the forward model calculation. These models gave GFR values of 7.2 to 8.8, with calculated density contrasts that ranged from  $403 \text{ kgm}^{-3}$ , for the entire uplift, to  $1266 \text{ kgm}^{-3}$  for a body consisting of about one-third of the edifice (i.e., one 500 m layer).

Models B1 through B6 were an attempt to see whether a buried cylindrical body might explain the residual anomaly. A density anomaly of this shape might be caused by the bottom of the guyot being buried by lower density sediments or even a dense volcanic plug beneath the guyot. Models E1 through E3 take this idea farther, using a cylinder with a denser conduit at its center (Fig. 9). For simplicity,

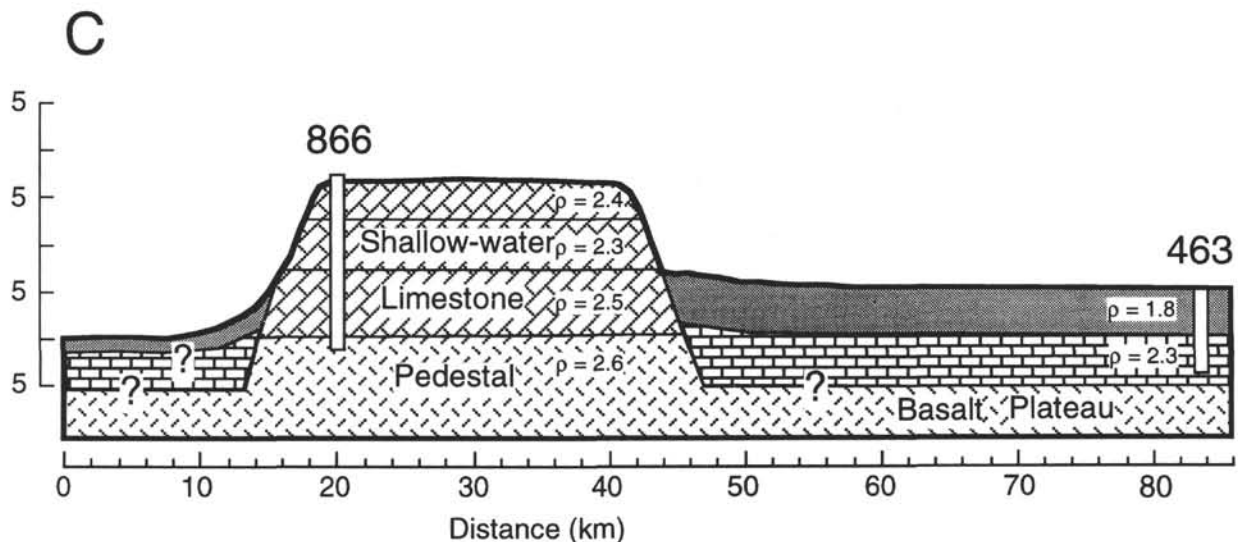


Figure 4 (continued).

the conduit was assumed to have twice the density contrast of the surrounding cylinder. These volcanic conduit models were tried because such dense regions have been observed and modeled in other seamounts (Kellogg and Ogujiofor, 1985; Kellogg et al., 1987) and are typical of the vent regions of Hawaiian Islands volcanoes (Strange et al., 1965).

Residual Models C1 through C6 and D1 assumed that the residual anomaly was produced by a buried conical seamount, perhaps consisting of basalt. The C models differ from Model D1 in that the former have the top of the bottom layer at either 3.0 km, the approximate depth that basalt was encountered in Hole 866A, or 2.5 km, the depth of the dolomitized zone above the basalt. The top and bottom of the cone were varied to determine the effect of volume and shallowness on the gravity model. The best fit of observed with calculated residual anomalies was given by Model C4, with a top at 2.0 km and bottom at 4.5 km (Table 1; Fig. 9). This could represent a buried seamount remnant whose top is 1.0 km above the level of the basalt at Site 866.

Other C series models fit the residual anomaly nearly as well as Model C4, but gave different density contrasts, which ranged from 256 to 685  $\text{kgm}^{-3}$  because of their differing volumes (Table 1). Model D1 fit the data nearly as well as Model C4, with a GFR of 12.7, and it gave a density contrast of 434  $\text{kgm}^{-3}$ . Of all these models, C2 through C6 and D1 are statistically indistinguishable, but Model C1 and Models A1 through A4 fit the data significantly worse.

## DISCUSSION

Drilling at Sites 866 and 463 provided a detailed record of the vertical density structure within and on the flanks of Resolution Guyot (Fig. 4). To use these densities for a model, it was necessary to assume horizontal layering, so that these parameters could be applied both to the edifice as a whole and to the surrounding sediment apron. Although seismic reflection profiles acquired over the guyot suggest some lateral variability within the shallow-water carbonates, perhaps owing to facies variations, the major density changes seem to be correlated with the gross layering, which can be traced across the guyot on seismic profiles (Sager, Winterer, Firth, et al., 1993). Likewise, seismic reflection profiles over the surrounding sediments show nearly horizontal layers (Thiede, Vallier, et al., 1981). Thus, the assumption of lateral density homogeneity should be reasonably good.

By modeling the residual anomaly with density contrasts that are buried just beneath the buildup, the assumption has been made that deeper density contrasts do not affect the local gravity anomaly sig-

nificantly. Of all subsurface density interfaces, that most likely to violate this assumption is the Moho discontinuity. Furthermore, the depth and shape of the Moho is dependent on a seamount's isostatic compensation, which can vary considerably.

Kellogg and Ogujiofor (1985) found that the free-air anomaly over Sio Guyot, in the western Mid-Pacific Mountains (Fig. 1), is much smaller than expected from its large volume because its topography has been completely compensated by a depressed Moho. Several observations suggest that Resolution and Heezen guyots are also likely to have been completely compensated. First, Resolution Guyot is near the age of the underlying lithosphere (Sager, Winterer, Firth, et al., 1993), so it and the plateau on which it sits should have formed when the lithosphere had a small elastic thickness. Second, the Mid-Pacific Mountains plateau beneath both guyots should be compensated because of its large size (Watts and Ribe, 1984). Lithospheric flexure modeling of several gravity lines over the Mid-Pacific Mountains indicate these features are indeed compensated (Watts and Ribe, 1984). Nevertheless, the Moho was not explicitly modeled in this study because Resolution Guyot is located in the middle of a section of plateau, over 50 km from its edges (Fig. 1); thus, the compensating root and its gravity anomaly are likely to be much wider than the modeled gravity anomaly. This assumption may not be as applicable to Heezen Guyot because this feature is located near the edge of the plateau (Fig. 1). Indeed, the larger gradient on the west side of this guyot's free-air anomaly (Fig. 3B) may be an effect of the plateau edge.

Although the forward gravity model of the Resolution Guyot buildup is well constrained owing to the density data provided by drilling, the lack of deep subsurface density control makes the inverse model nonunique. The subsurface modeling approach was first to define the lateral shapes and sizes of anomalous masses based on locations of expected or observed density contrasts within or below the guyot. Subsequently, the top and bottom depths of the bodies were varied to examine the effect of changing the volume. As the analysis showed (Table 1), a variety of different models can adequately reproduce the residual gravity anomaly. Nevertheless, many of these models can be rejected because they give densities or dimensions that are unrealistic.

Models A1 through A4 placed the excess mass within one or more of the carbonate buildup layers above the seafloor (Fig. 9). This was to see whether the mass excess can be explained by incorrect densities assigned to layers in the forward model. Despite the fact that all of these models fit the data reasonably well, they must be rejected because their density contrasts, 403 to 1266  $\text{kgm}^{-3}$ , are unacceptably high. Adding these values to the density contrasts used in the forward

Table 1. Residual gravity anomaly model parameters.

ID	Description	Density contrast ( $\text{kgm}^{-3} \pm 2\sigma$ )	Depth (km)	GFR <sup>a</sup>	Variance	Variance 95% confidence limit <sup>b</sup>	
A1	Carbonate uplift (all)	403	$\pm 40$	1.3–2.65	7.2	2.5	6.9
A2	Carbonate uplift (bottom 900 m)	609	$\pm 72$	1.75–2.65	6.3	6.1	1.7
A3	Carbonate uplift (dolomite section)	1266	$\pm 222$	2.25–2.65	4.9	6.5	5.8
A4	Carbonate uplift (450 m layer at top)	1111	$\pm 88$	1.3–1.75	8.8	8.7	1.7
B1	Narrow cylinder <sup>c</sup>	664	$\pm 60$	3.0–4.5	7.3	11.1	5.0
B2	Wide cylinder <sup>d</sup>	395	$\pm 26$	2.0–3.5	9.9	6.6	8.9
B3	Wide cylinder <sup>d</sup>	1238	$\pm 84$	2.5–3.0	9.9	6.6	8.9
B4	Wide cylinder <sup>d</sup>	628	$\pm 42$	2.5–3.5	10.2	6.3	8.5
B5	Wide cylinder <sup>d</sup>	468	$\pm 30$	3.0–4.5	10.4	6.0	8.1
B6	Wide cylinder <sup>d</sup>	300	$\pm 20$	3.0–5.5	10.3	6.0	8.1
C1	Seamount <sup>e</sup>	685	$\pm 44$	2.0–3.5	9.8	6.2	8.4
C2	Seamount <sup>f</sup>	529	$\pm 28$	2.0–3.5	12.2	4.4	5.9
C3	Seamount <sup>e</sup>	475	$\pm 24$	2.0–4.0	12.2	4.2	5.7
C4	Seamount <sup>e</sup>	365	$\pm 18$	2.0–4.5	12.8	4.0	5.4
C5	Seamount <sup>e</sup>	256	$\pm 14$	2.0–5.5	12.6	4.2	5.7
C6	Seamount <sup>e</sup>	419	$\pm 22$	2.0–4.5	12.1	4.5	6.1
D1	Deep seamount	434	$\pm 22$	3.0–5.5	12.7	4.1	5.5
E1	Cylinder <sup>d</sup>	545	$\pm 28$	2.5–3.5	12.5	4.3	5.8
	+ conduit <sup>g</sup>	1090	$\pm 56$	2.5–3.5			
E2	Cylinder <sup>d</sup>	1170	$\pm 124$	3.0–3.5	12.3	4.4	5.9
	+ conduit <sup>g</sup>	2340	$\pm 248$	3.0–3.5			
E3	Cylinder <sup>d</sup>	408	$\pm 44$	3.0–4.5	12.5	4.3	5.8
	+ conduit <sup>g</sup>	816	$\pm 88$	3.0–4.5			
E4	Cylinder <sup>d</sup>	262	$\pm 28$	3.0–5.5	12.4	4.4	5.9
	+ conduit <sup>g</sup>	524	$\pm 56$	3.0–5.5			

<sup>a</sup> GFR = Goodness-of-fit ratio (mean observed anomaly divided by mean residual anomaly [observed minus calculated gravity]).

<sup>b</sup> Variance 95% confidence limit; if variance of another model is larger than this number (for same or nearly same number of observation points), then model fits data significantly worse with 95% confidence (using an F-test on variance ratios, assuming errors with Gaussian distribution).

<sup>c</sup> Middle layer of residual model (Fig. 6).

<sup>d</sup> Bottom layer of residual model (Fig. 6).

<sup>e</sup> Top of bottom layer at 3.0 km depth.

<sup>f</sup> Top of bottom layer at 2.5 km depth.

<sup>g</sup> Top layer of residual model (Fig. 6).

model implies densities of in excess of  $2800 \text{ kgm}^{-3}$ , but limestones are not so dense.

The B models were vertical, nearly cylindrical prisms (Fig. 9) of varying dimensions. Model B1 used a cylindrical body narrower than the guyot (the middle layer of the model in Fig. 6B) to see if such a body could mimic the residual anomaly. This model fit the anomaly poorly (Fig. 9), indicating that the mass excess must be close to the same width as the guyot, if it is to be in the shallow subsurface.

Models B2 through B6 used a cylinder the same width as the guyot (the bottom layer of the model in Fig. 6B). This could represent, for example, the contrast between dense, dolomitized limestone in the bottom 417 m of Hole 866A vs. the surrounding low density sediments as well as the contrast between the basalt pedestal and surrounding limestones (Fig. 4). These models provided close fits to the residual anomaly, with GFR values in excess of 9.9. The contrast between the dolomites and surrounding sediments is approximately  $700 \text{ kgm}^{-3}$  ( $1800 \text{ kgm}^{-3}$  vs.  $2500 \text{ kgm}^{-3}$ ), whereas the contrast between basalt and surrounding limestones is about  $300 \text{ kgm}^{-3}$  ( $2600 \text{ kgm}^{-3}$  vs.  $2300 \text{ kgm}^{-3}$ ). This suggests that the average should be approximately  $480 \text{ kgm}^{-3}$  (400 m of dolomite and 500 m of basalt). Model B3 gave a density contrast of  $1238 \text{ kgm}^{-3}$ , which is much too large. Model B4, with a contrast of  $628 \text{ kgm}^{-3}$  is also somewhat large, even though it spans the expected depths for the dolomite and basalt pedestal (Fig. 4). Models B2, B5, and B6 give lower density contrasts, but at the expense of having a top shallower than expected (B2) or a bottom deeper than expected (B5, B6). If Model B2 is accepted, dense material is about 500 m shallower than indicated by Site 866 density data and, therefore, these data must not be representative of the guyot. On the other hand, Models B5 and B6 imply that the mass excess extends deeper than the predicted top of the basalt plateau beneath the guyot (3.5 km). It is possible, therefore, that the extrapolated depth of the top of the plateau is erroneous, particularly if acoustic "basement" in seismic profiles over the plateau is not the limestone/basalt contact as supposed.

Although the wide cylinder models fit more than 90% of the residual gravity anomaly, they predict a lesser residual over the center of the guyot than was observed. This can be remedied by adding excess mass to the center of the residual model. Two different types of models were tried to address this inadequacy. One type, Models C1 through C6 and D1, add two narrower layers on top of the wide cylinder used previously (Figs. 6, 9). This model can represent a more-or-less conical seamount beneath the guyot, rather than a flat pedestal. The second type, Models E1 through E4, place the excess mass in a narrow vertical pipe within the cylinder used previously (Fig. 9). This model can represent a dense intrusive igneous conduit or feeder, as has been modeled in other seamounts (Kellogg and Ogujiofor, 1985; Kellogg et al., 1987). With the exception of Model C1, all the other models give GFR values in excess of 12.2, indicating that more than 93% of the residual has been matched. Although the difference in the anomaly fits between these models and the simple cylinder models seems small, variance analysis indicates that the models with central mass concentrations fit significantly better (Table 1).

As before, some of these models can be ruled out owing to unreasonable densities or dimensions. Model C1 gives a density contrast,  $685 \text{ kgm}^{-3}$ , that is likely too high. Models C1 through C4 demonstrate a space problem. If the top of the main, bottom layer is to be at 3.0 km, the basalt/limestone interface depth, or at 2.5 km, the top of the dolomitized zone, there is little space above for a cone. These models have summits at a depth of 2.0 km, but this is only about 640 m below the summit of the guyot. If a basaltic cone rises to this height inside the guyot, it would likely have been detected by seismic reflection profiles. However, if its top depth were 2.5 km, as in Model C5, it could be hidden within the dense dolomitized zone. In addition, as with some of the cylinder models, Models C3 through C6 have their bases below the predicted top of the plateau, implying a density contrast within it. This is especially so for Model D1, which is a conical seamount with its top at 3.0 km and the top of the main,

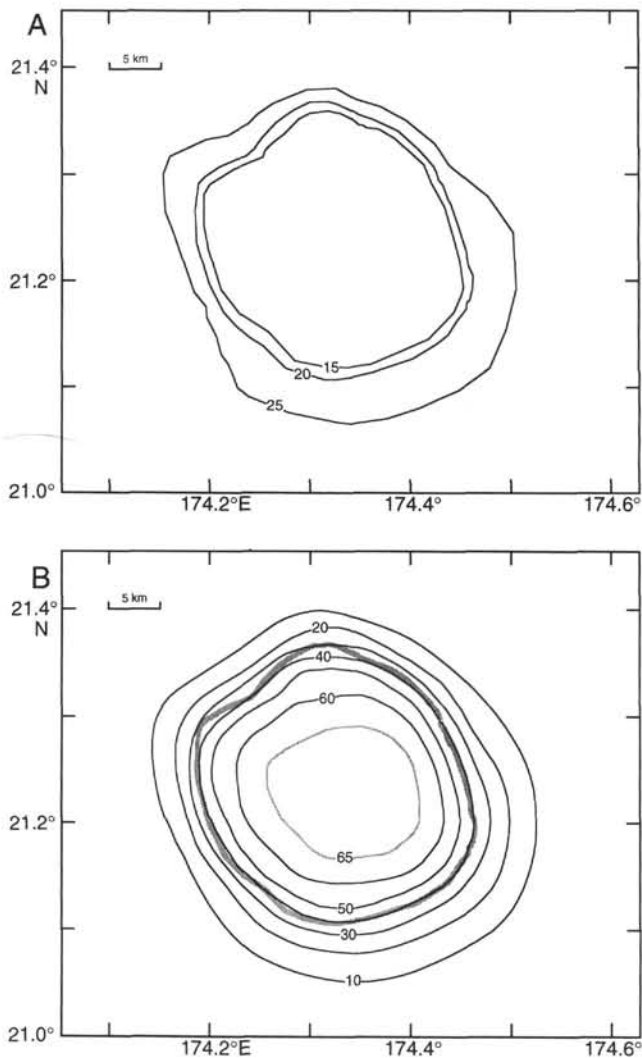


Figure 5. Bathymetry model (A) and calculated free-air anomaly (B) of Resolution Guyot. Lines on the model map represent the vertical sides of polygonal prisms used to represent the bathymetry (Plouff, 1976). These are labeled by the depths of the bathymetry contours (in hundreds of meters) used to constrain their shape. Calculated free-air anomaly contours are shown at 10-mGal levels, except for the 65 mGal contour, which is shown in gray. The heavy gray contour shows the 2000-m bathymetry contour.

bottom layer at 4.0 km, approximately 1 km deeper than the basalt/limestone contact. This particular model is implausible because it does not account for the known large density contrasts, in favor of deeper, unconstrained contrasts.

Models E1 through E4 use the same wide vertical cylinder as the B models, but have the extra central mass within this cylinder in the form of a narrower, vertical, cylindrical conduit zone with twice the density contrast (Fig. 9). The density contrast doubling is the effect of inverting for a single, average density contrast, but having the narrow cylinder within the wide cylinder. Because this situation is contrived, the density contrasts of the conduit in Table 1 should be treated with some skepticism. Models were tried in which the densities of the two bodies were allowed to vary independently, but the result was that the uncertainty in the density contrast of the smaller body was large owing to the fact that it is constrained by a very small portion of the residual.

If the mass anomaly of the E models is compressed into a thin layer, as in Model E2, the resulting density contrast is implausibly high ( $1170 \text{ kgm}^{-3}$ ). Likewise, Model E1 yielded an average density contrast,  $545$

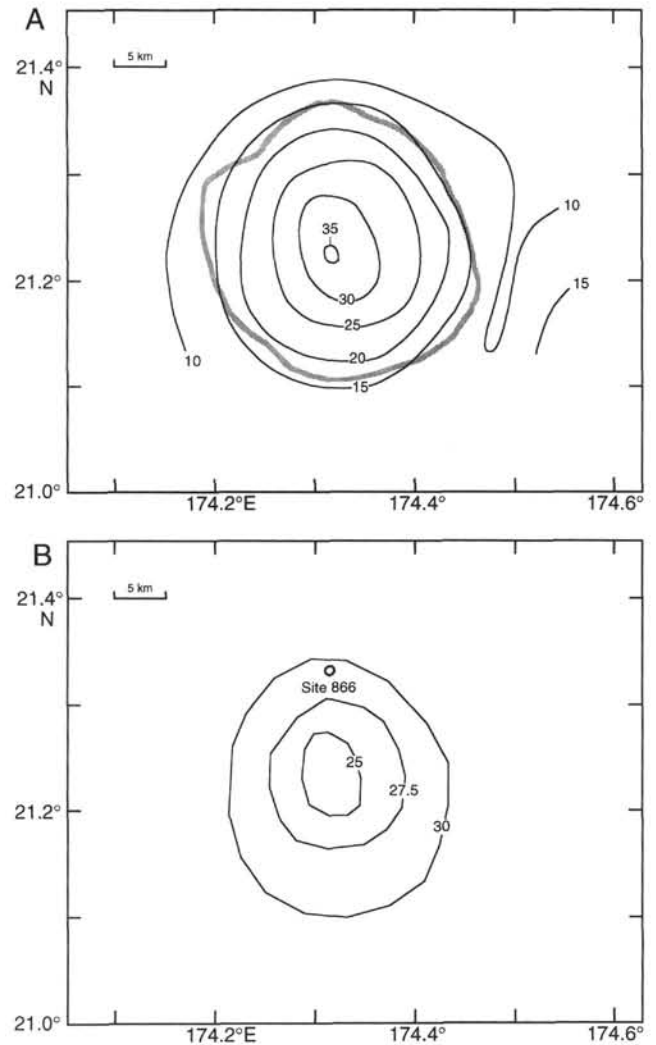


Figure 6. Resolution Guyot residual gravity anomaly (A) and residual mass anomaly model (B) for the residual gravity anomaly. The residual anomaly was determined by subtracting the calculated gravity anomaly (Fig. 5) from the observed anomaly (Fig. 2). Anomaly contours are shown at 5-mGal intervals and labeled in mGal. Heavy gray contour shows the 2000-m bathymetry contour. Polygons in B represent the vertical edges of prisms used for the gravity model calculations (Plouff, 1976). Contours are labeled by depths used in Model C6 (Table 1). Location of Site 866 shown by open circle.

$\text{kgm}^{-3}$ , that is probably slightly too high, even though it occupies the depth ranges in which the greatest density anomalies are expected (i.e., 2.5 to 3.5 km). Models E3 and E4 gave lower, more plausible density contrasts, but these models have bottoms below the expected plateau top depth (3.5 km). Although statistically indistinguishable from the buried seamount models, the cylinder/conduit models may be more plausible because there is no problem of where to place the excess mass within the seismically imaged part of the guyot.

To summarize the Resolution Guyot modeling results, it is clear that the excess mass indicated by the residual is caused by a shallow density contrast that is at or below the level of the seafloor surrounding the guyot. Models that attribute the excess mass to the buried dolomitized zone and basalt pedestal, surrounded by sediments of lesser densities, can account for much of the residual anomaly. Models with a central concentration of excess mass, such as a buried basaltic erosional remnant or a conduit filled with dense intrusive igneous rock, fit the residual significantly better than those without. Given the space problem attendant with the former model type, the

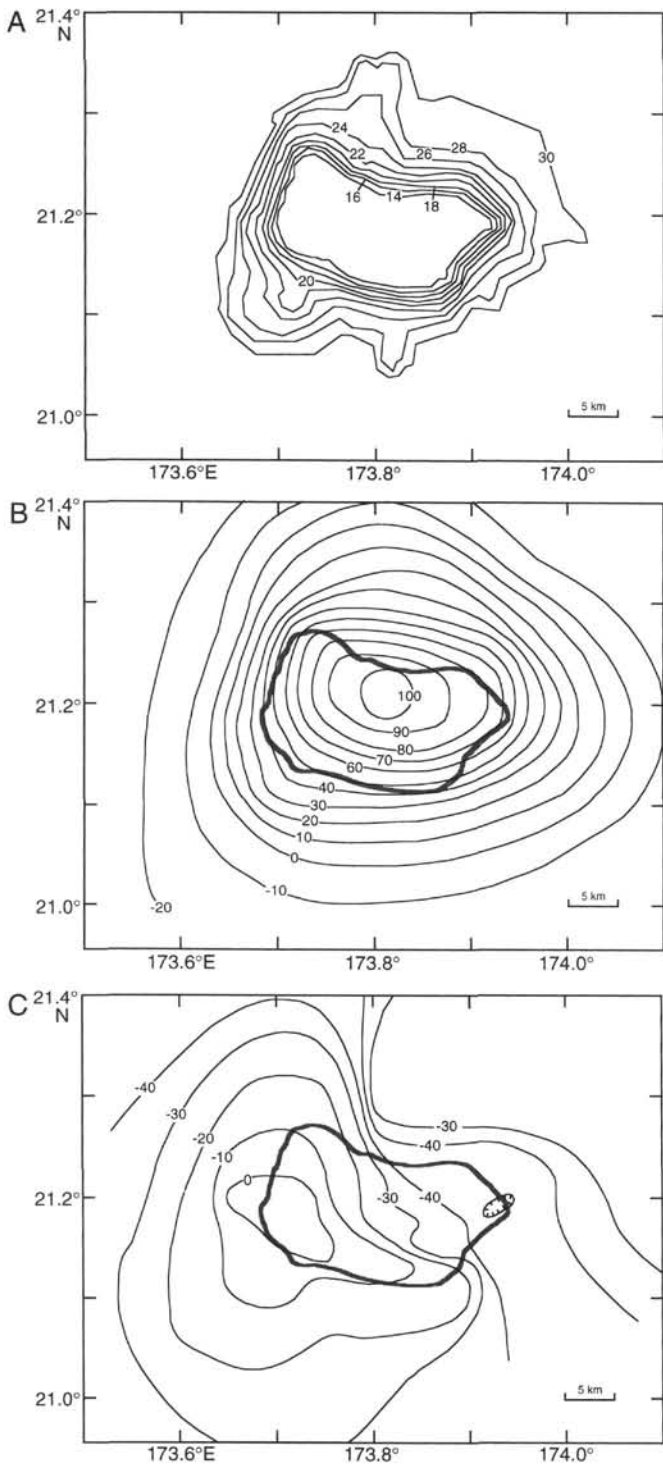


Figure 7. Bathymetry model (A), calculated topographic gravity anomaly (B), and residual gravity anomaly (C) of Heezen Guyot. The residual was determined by subtracting the calculated gravity anomaly (B) from the observed free-air anomaly (Fig. 3). Conventions as in Figure 5.

latter type seems more plausible. In addition, if the excess mass is restricted to the depth zone between the top of the dolomitized limestones and the predicted top of the basalt plateau beneath the guyot, the average density contrast is slightly higher than expected. Models with bottoms somewhat deeper than the plateau top give more realistic density contrasts and may indicate that there is a denser zone

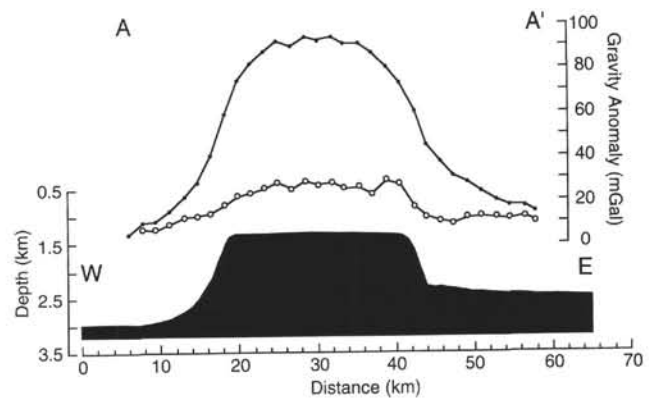


Figure 8. Free-air and residual gravity anomaly profiles over Resolution Guyot. Observed anomaly is shown by filled circles; residual anomaly, by open circles. At bottom is a bathymetry profile that corresponds to the same line. Vertical exaggeration is approximately 7:1. Profile beginning and end points are shown by A–A' in Figure 1. Note that the profile is not a straight line, and the small spike in the residual anomaly, at approximately 40 km on the east side of the guyot summit, is an artifact resulting from a change in ship's course.

within the plateau beneath the guyot or that the estimate of the depth of the plateau top is in error by approximately 500 m to 1000 m.

The gravity residual of Heezen Guyot was not modeled because (1) it is similar to that of Resolution Guyot, thus, the results would be alike, and (2) there are no density data for constraints of its model. Nevertheless, the similarity in amplitude and shape of the Heezen Guyot residual compared with that of Resolution Guyot implies that a similar density anomaly underlies this guyot as well. If the residual outlines the shape of an underlying basalt pedestal, the dissimilarity of the guyot's bathymetric shape and its residual gravity anomaly suggest that the carbonate bank expanded eastward from its pedestal and is roughly twice as large in area as the basalt feature.

## CONCLUSIONS

Free-air gravity anomalies over Resolution and Heezen guyots have amplitudes of 100 and 140 mGal, respectively. Subtracting the effects of the carbonate uplifts of each guyot, constrained by density data from Hole 866A cores and logs, leaves a residual anomaly over each guyot. For Resolution Guyot, this residual is subcircular, like the guyot, positive, centered over the edifice, and with an amplitude of 35 mGal. The residual for Heezen Guyot is similar in amplitude, 45 mGal, and in shape, but is located over the western side of that feature.

A series of models of the Resolution Guyot residual anomaly showed that the excess mass cannot be explained by a reasonable error in the densities used for the model of the carbonate edifice. These models also show that the excess mass must have a width approximately equal to that of the carbonate edifice. Most of the excess mass can be attributed to the contrast between the dense dolomitized limestone section and underlying basalt pedestal relative to sediments surrounding the guyot. Nevertheless, models that have a mass concentration in the center and a bottom below the expected top of the underlying basalt plateau give better results. The central mass concentration may be either a buried basaltic cone within the guyot or a relict conduit filled with dense intrusive rocks. The latter seems more probable because the former should have been detected by seismic profiles over the edifice. Models with bottoms deeper than the expected top of the plateau give more reasonable average density contrasts and suggest that either a mass excess exist within the plateau or the top depth of the plateau, which has been extrapolated from acoustic "basement" on seismic reflection profiles, may be incorrect. The models suggest that the carbonate bank grew atop a small pedestal beneath Resolution Guyot and retained its horizontal shape and

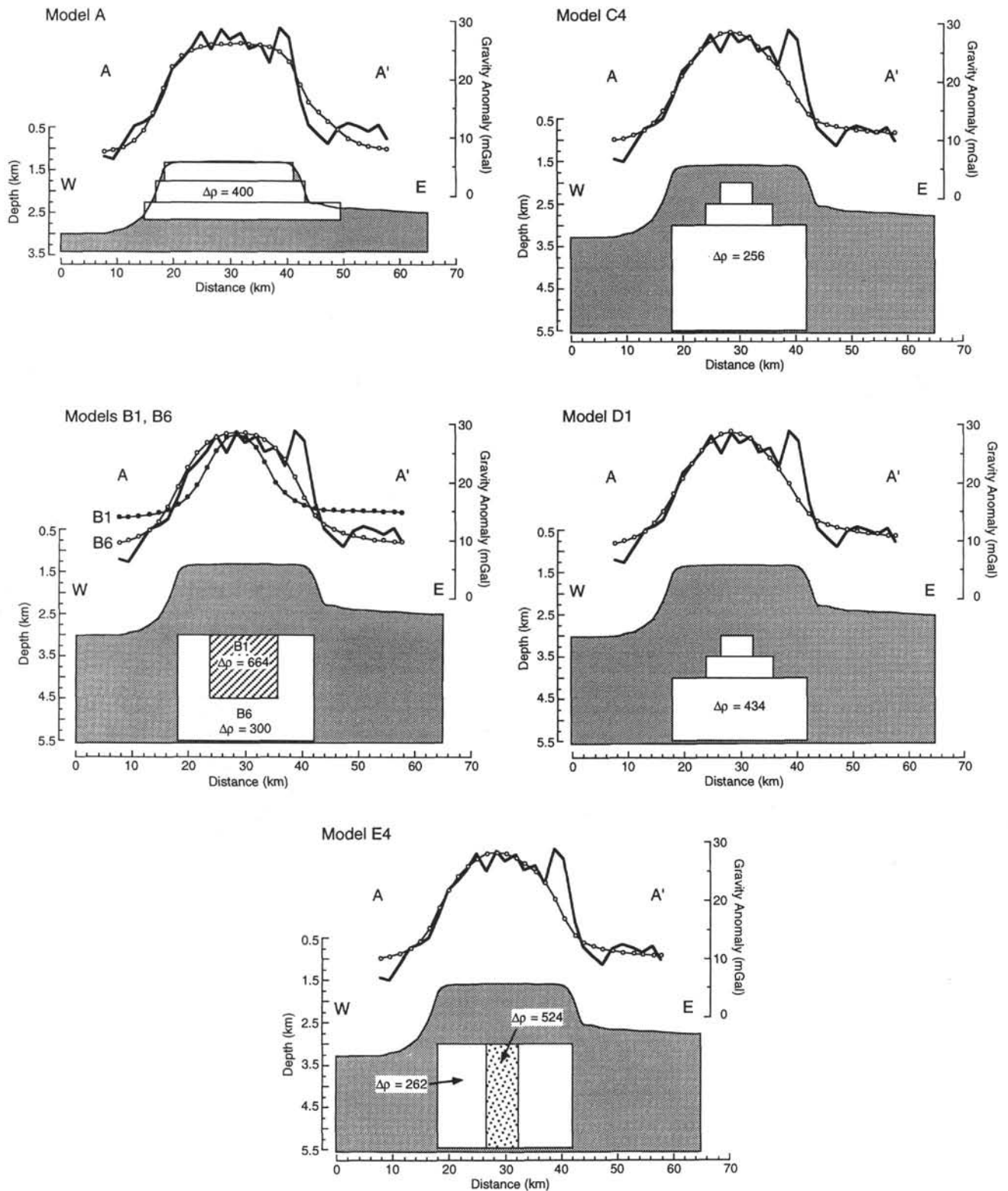


Figure 9. Comparison of observed with calculated residual gravity anomalies for various inverse models of the mass anomaly beneath Resolution Guyot. Model identifiers correspond to those in Table 1. At the top of each plot are curves representing the observed residual anomaly (heavy solid line) and the calculated anomaly (light solid line with open or filled circles). A representation of the modeled mass anomaly bodies is shown below each set of curves in relation to a bathymetric profile. The anomaly curves and bathymetry profiles are along A–A', shown in Figure 1. In the lower left panel, Model B6 is represented by the curve with open circles and the white body; Model B1, with filled circles and hachured body. Note that the spike in the residual anomaly profile at approximately 40 km, on the east side of the guyot summit, is an artifact caused by a change in ship's course.

dimensions. However, the residual anomaly of Heezen Guyot implies the carbonate bank that built that edifice expanded significantly from the original subcircular seamount.

### ACKNOWLEDGMENTS

The author thanks the Captain, crew, and scientific staff of the research vessels *Thomas Washington* and *JOIDES Resolution*, who made the collection of gravity and bathymetry data possible. In particular, the author is indebted to Jeroen Kenter and Michael Ivanov, who made meticulous shipboard sample density measurements, and to the Lamont-Doherty Earth Observatory Borehole Research Group, who acquired the log density measurements. The JOI/USSAC science support program provided the funds for this study. Reviews by James Kellogg and Albert Rudman led to significant improvements in the manuscript. This is Texas A&M Geodynamics Research Institute Contribution No. 095.

### REFERENCES\*

- Bell, R.E., and Watts, A.B., 1986. Evaluation of the BGM-3 sea gravity meter system on board R/V *Conrad*. *Geophysics*, 51:1480–1493.
- Bevington, P.R., 1969. *Data Reduction and Error Analysis for the Physical Sciences*: New York (McGraw-Hill).
- Freitag, H.C., 1987. Gravity fields of eight North Pacific seamounts: implications for density [M.S. thesis]. Texas A&M Univ., College Station, TX.
- Kellogg, J.N., and Ogujiofor, I.J., 1985. Gravity field analysis of Sio Guyot: an isostatically compensated seamount in the Mid-Pacific Mountains. *Geo-Mar. Lett.*, 5:91–97.
- Kellogg, J.N., Wedgeworth, B.S., and Freymuller, J., 1987. Isostatic compensation and conduit structures of western Pacific seamounts. In Keating, B.H., Fryer, P., Batiza, R., and Boehlert, G. (Eds.), *Seamounts, Islands, and Atolls*. Geophys. Monogr., Am. Geophys. Union, 43:85–96.
- LePichon, X., and Talwani, M., 1964. Gravity survey of a seamount near 35°N 46°W in the North Atlantic. *Mar. Geol.*, 2:262–277.
- Mammerickx, J., and Smith, S.M., 1985. *Bathymetry of the North Central Pacific*. Geol. Soc. Am., Map and Chart Ser., MC-52.
- Plouff, D., 1976. Gravity and magnetic fields of polygonal prisms and application to magnetic terrain corrections. *Geophysics*, 41:727–741.
- Sager, W.W., Davis, G.T., Keating, B.H., and Philpotts, J.A., 1982. A geophysical and geologic study of Nagata Seamount, northern Line Islands. *J. Geomagn. Geoelectr.*, 34:283–305.
- Sager, W.W., Winterer, E.L., Firth, J.V., et al., 1993. *Proc. ODP, Init. Repts.*, 143: College Station, TX (Ocean Drilling Program).
- Schimke, G.R., and Bufe, C.G., 1968. Geophysical description of a Pacific Ocean seamount. *J. Geophys. Res.*, 73:559–569.
- Strange, W.E., Woollard, G.P., and Rose, J.C., 1965. An analysis of the gravity field over the Hawaiian Islands in terms of crustal structure. *Pac. Sci.*, 19:381–389.
- Thiede, J., Vallier, T.L., et al., 1981. *Init. Repts. DSDP*, 62: Washington (U.S. Govt. Printing Office).
- Watts, A.B., and Ribe, N.M., 1984. On geoid heights and flexure of the lithosphere at seamounts. *J. Geophys. Res.*, 89:11152–11170.
- Winterer, E.L., and Metzler, C.V., 1984. Origin and subsidence of guyots in Mid-Pacific Mountains. *J. Geophys. Res.*, 89:9969–9979.

\*Abbreviations for names of organizations and publications in ODP reference lists follow the style given in *Chemical Abstracts Service Source Index* (published by American Chemical Society).

**Date of initial receipt: 29 November 1993**

**Date of acceptance: 6 July 1994**

**Ms 143SR-251**